

USE OF CFD TO PREDICT THE PERFORMANCE OF A HEAT TREATMENT FURNACE

Yongxiang YANG¹, Reinier A. de JONG¹ and Markus A. REUTER¹

¹Resource Engineering, Department of Geotechnology, Delft University of Technology
Mijnbouwstraat 120, 2628 RX, Delft, The Netherlands

ABSTRACT

In this paper, a mobile heat treatment furnace was simulated by using CFD to investigate thermal performance of the furnace and the heating process of the metal pieces. The furnace is used to heat treat dredging pumps and impellers to obtain the required microstructure and mechanical properties through stress relief, annealing, hardening and tempering. Since the temperature evolution inside the metal piece cannot be tracked in practice, CFD simulation provides a useful tool to predict the temperature evolution within the metal pieces during the heat treatment. The current CFD model consists of turbulent combustion, thermal radiation, and conjugate heat transfer. Temperature measurement was carried out to provide thermal boundary conditions and calibrate model parameters. An overall energy balance indicated a relatively low energy efficiency of the furnace. To improve energy efficiency design changes were made with the model. Reducing the amount of excess air will also save a lot of energy and thus cost in production. Heating of the furnace by means of radiation plates proved to be a good alternative.

Keywords: dredging impeller, transient heating, heat treatment, CFD simulation.

INTRODUCTION

Heat treatment is a common practice in metal production and manufacturing industries. Through heat treatment at certain temperatures with special patterns, unique mechanical properties of the metals and the metallic products could be obtained. At Akkermans Gloeitechniek, a Dutch company situated in Kinderdijk, (a sub-contractor of IHC-Holland) heat treatment of metal components for dredging industry is conducted for various type of heat treatment such as stress relieving, soft annealing and hardening, tempering, transformation and precipitation. At the company 6 furnaces are in operation and the 7th is being built.

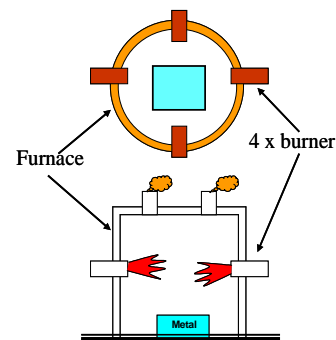
One of the furnaces is a mobile cylindrical one, as shown in Figure 1. The process is based on changes in the crystal structure of the metals. For example, for hardening treatment material is heated up slowly up to around 1000°C. At this temperature the structure of steel changes into "austenite". After rapid cooling (remove the hood) the steel becomes much harder. Cooling can be done in air, in water, and in oil or polymers. The furnace is heated up by oil-burners. Temperature control is done with thermocouples and controllers. When the temperature becomes too high, the controller gives a signal to the burners, which turn off at that time. When the temperature becomes too low, the burners are

turned on by the controller. The controller works with a set point and a process value, as PID controllers. The result of the temperature profile is printed on paper. After this a hardness measurement is made to check whether the results are all right.

At the moment problems with heating of impellers used in dredging pumps occur. The hardness of the impeller is not uniform; in the middle the material is much thicker, which causes it to cool down more slowly. The hardness at this point is lower. To get a better understanding of the heating and cooling of these impellers a computer model would be very useful. This will lead to a better controlled process, significant energy savings and more environmental friendly production.



(a) The mobile furnace



(b) burner orientation

Figure 1: The mobile heat treatment furnace and the schematic view.

THE HEAT TREATMENT PROCESS

The heating process starts with placing the metal piece on supporting bricks. This is done to support the metal so that it would not plastically deform at high temperatures or even break in two pieces. When the metal piece is placed on the support the contact thermocouples are attached to the metal and connected to the controller unit and indirectly to the recording unit. The mobile furnace is placed on top of the metal as a hood. Sand is pushed to the sides of the furnace to seal it better. After the burners are connected to the controlling unit the heating profile is inserted into the controller. Time and temperature are set to give a heating profile along the heating process, as is illustrated in Figure 2. Heating rate, intermediate soaking time and end soaking time can be set. When all this is done the program can start and the furnace is in operation. The heating process is automatically controlled so that no manual changes are necessary.

After the heating up and soaking stages, which take around twenty hours, the burners are disconnected from the controller and the hood is removed to let the metal cool down. The metal piece at about 980°C cools down to environmental temperature in open air. After the metal is completely cooled down, usually the next day, the hardness of the metal is measured at different points to check whether the process was successful. Table 1 lists the general operation data of the heat treatment process, including overall mass and energy balance.

The energy distribution in the furnace varies a lot along the operation as will be illustrated from the model results later. For instance, the heat loss from the walls and the energy carried out from the off-gas are lower in the beginning than in the end, while the energy stored in the metal piece becomes smaller along the heating process. This is a time-dependent dynamic process.

Item	Average value
Furnace dimension:	
Inner diameter × Height × Lining thickness	3.76 × 3.50 × 0.12 m
Burner inner diameter and location	0.1 m, 1.5 m from furnace bottom
Average fuel consumption	37.18 kg/hr
Average air supply	1327.2 kg/hr
Stoichiometric ratio	17.24
Average excess air	107%
Average wall temperature	50°C
Average off gas temperature	668°C
Average weight of the impeller	4,620 kg

Table 1: Operating data of a typical heat treatment operation.

CFD SIMULATION

Simulation Tool

The heat treatment process in the furnace involves turbulent gas flow, oil combustion, thermal radiation and conjugate heat transfer within the metal components and furnace walls. The simulation is conducted by using a general purpose CFD

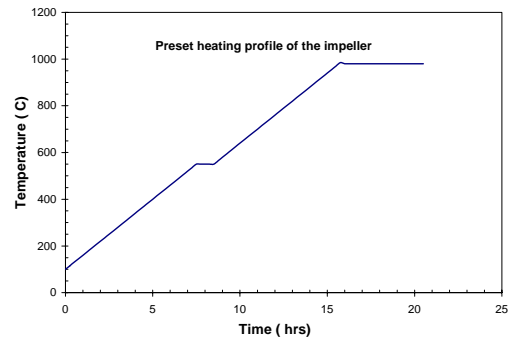


Figure 2: The preset heating profile of the dredging impeller.

package PHOENICS 3.5 (Cham, 2004). The governing partial differential equations for conservation of mass, momentum, and energy in a turbulent flow system can be expressed by time-averaged 2nd order partial differential equations as is shown in equation (1), and solved with a common numerical algorithm in the code.

$$\frac{\partial}{\partial t}(\rho\phi) + \text{div}(\rho\mathbf{u}\phi) = \text{div}(\Gamma_{\phi,eff} \text{grad}\phi) + S_{\phi} \quad (1)$$

Where ϕ is the general flow variable such as velocity components, temperature and mass fractions of chemical species; ρ is the fluid density; \mathbf{u} is the fluid velocity vector. The effects of fluid turbulence are accounted for in the transport coefficient $\Gamma_{\phi,eff}$ by a turbulence model, and S_{ϕ} is a general source term which could include all terms other than transient, convection and diffusion terms in the equation. In the current simulation, all the above mentioned transport processes are modelled as below:

- Turbulence: the standard $k-\epsilon$ model
- Thermal radiation: IMMERSOL (Immersed solid)
- Oil combustion: global gas combustion model (simplified from oil to gaseous fuel)

The global gas combustion model and the immersed solid radiation model are described in more detail later. Since the general information about the standard $k-\epsilon$ turbulence model is available for most CFD analysts and process engineers, it is not be described in this paper. Some preliminary simulation results have been published previously (Yang et al., 2004). The current paper describes new developments and findings. More details of the results can be found in the MSc. Thesis of de Jong (2004).

Global Combustion Model (SCRS)

As the first approximation, the oil combustion is simplified with gas combustion model. Based on the oil properties, the same amount of gaseous fuel with the same heat of combustion is estimated. The oil is assumed to vaporize immediately upon entering the furnace.

In PHOENICS, the global gas combustion model developed by Spalding (1979) was implemented as the Simple Chemically Reaction System (SCRS). The SCRS involves a

reaction between two reactants (fuel and oxidant) in which these combine, in fixed proportions by mass, to produce a unique product:

$$1 \text{ kg fuel} + s \text{ kg oxidant} = (1+s) \text{ kg product} \quad (2)$$

Where s is the stoichiometric oxidant requirement (kg oxidant/kg mixture), ensuring complete combustion. This reaction is taken as irreversible. Reaction rates in turbulent flow situations are often more greatly affected by local turbulence than by chemical factors. For these situations the Eddy Break-up (EBU) model is provided, which rests on the hypothesis that only turbulence and fuel concentration affect the reaction rate having the following source term in the mass conservation equation:

$$S_{m_{fu}} = -CEBU \times \min\{m_{fu}, m_{ox}/s\} * \frac{EP}{KE} \quad (3)$$

Where CEBU is the Eddy Break-up reaction constant, m_{fu} is the mass fraction of unburned fuel, m_{ox} is the oxidant fraction, KE is the turbulent kinetic energy and EP the dissipation rate of KE. In the current study it is assumed that the reaction rate for the combustion of the oil vapor is turbulent mixing rate limited and the EBU is chosen to determine the reaction rate. The reaction rate constant in the EBU model proved to be an important parameter, and it generally determines the shape and size of the flame. Different CEBU values have been tested between 1 and 50. It was found that if the CEBU value is set below 25 no normally observed flame could be formed and the combustion takes place in the broader space in the furnace except in the normal flame zone. Thus the value of 25 has been finally used in the simulation model based on the observation of the flame shape and flame temperature.

Immersed Solid Radiation Model (IMMERSOL)

Thermal radiation plays a critical role for combustion furnaces and the heat transfer between the combustion gases and the metal components. Many radiation models have been developed in the world, and in PHOENICS three radiation models for participating media are available: the 6-flux model, radiosity model, and the immersed solid model (IMMERSOL) ^[1]. Since its special design to handle conveniently the multi-solid flow domain and the conjugate heat transfer with conducting solids, it has been chosen for the current study.

The IMMERSOL model is a single heat-conduction-type equation that describes the influences of heat conduction within the solids and radiation in fluid domain between the solids on the distribution of immersed-solids temperature. The model is mainly dependent on position and conductivity of immersed-solids. This model is very useful for conjugate heat transfer problems such as the temperature distribution within the metal components. The IMMERSOL radiation model can be described with the differential equation within the immersed solid per unit volume as in Equation (4).

During simulation of the impeller heating there is no internal heat generation, so that q' becomes zero. Equation (4) means that radiation from a furnace wall and combustion gases will

be stored by the metal component. The radiance temperature T_3 is the temperature of the solid (the dredging impeller and the brick lining).

$$\frac{\partial}{\partial x} \left(k_1 \frac{\partial T_3}{\partial x} \right) + \frac{\partial}{\partial y} \left(k_1 \frac{\partial T_3}{\partial y} \right) + \frac{\partial}{\partial z} \left(k_1 \frac{\partial T_3}{\partial z} \right) + q' = C_p \frac{dT_3}{dt} \quad (4)$$

where: C_p specific heat capacity of the solid
 k_1 thermal conductivity of the solid
 q' the heat source per unit volume
 T_3 temperature of the solid

Within the space between the dredging impeller and furnace walls, the distribution of radiation temperature derived from radiosity ($E_3 = \sigma(T_3)^4$), can be represented as obeying the equation:

$$\frac{\partial}{\partial x} \left(k_2 \frac{\partial T_3}{\partial x} \right) + \frac{\partial}{\partial y} \left(k_2 \frac{\partial T_3}{\partial y} \right) + \frac{\partial}{\partial z} \left(k_2 \frac{\partial T_3}{\partial z} \right) = (a+s)\sigma(T^4 - T_3^4) \quad (5)$$

where: k_2 Temperature dependent conductivity of the fluid medium, and defined as

$$k_2 = \frac{16\sigma T_3^3}{3(a+s+1/WGAP)}$$

 T_3 radiation temperature of the fluid
 σ Stefan Boltzmann constant ($5.67 \times 10^{-8} \text{ W/m}^2 \cdot \text{K}^4$)
 T temperature of the fluid phase
 a absorptivity of the fluid medium
 s scattering coefficient of fluid medium
 WGAP distance between adjacent walls or from the metal component

Equation (5) means that the gas radiation is described in terms of conduction. The radiation temperature between the metal components or refractory walls can be computed at each location in the domain. The net contribution due to thermal radiation to the energy conservation equation (the energy source term in equation (1), S_ϕ) is the right-hand-side term in equation (5): $(a+s)\sigma(T^4 - T_3^4)$. Therefore, conduction type of equations (4) and (5) could describe the influences of both conduction in solids and gas-phase radiation between the solids on the immersed-solids temperature T_3 throughout the domain, with a position- and T_3 -dependent conductivity.

Geometry and Computational Grid

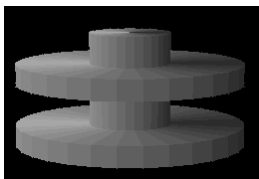
The model is constructed with Cartesian grid in order to get fast convergence. The PHOENICS VR-Editor, the pre-processor provide the flexibility to construct various shapes of objects with reasonable accuracy, without using BFC grid or unstructured grid system. In order to construct the furnace refractory wall and ceiling, high conducting solids embedded in refractory blocks (wall and ceiling) are used to form an internal cylindrical surface of the furnace and constant outer surface thermal boundary condition. In order to test grid

independence of the simulation, both coarse and fine grids are used. For the dredging impeller to be heat treated, both simplified impeller and the detailed impeller supplied with CAD design are used in simulation. Figure 3 shows the photo of the impeller and the simplified impeller as well as the CAD figure used in the model.

The coarse grid has number of 15,625 cells (25×25×25) and the finer grid has 125,000 cells (50×50×50) for the simplified impeller models. The model with the detailed dredging impeller consists of 187,974 cells (59×59×54). Figure 4 illustrates the computational grid for the detailed impeller model. The simulation results from both coarse and fine grid showed minor difference. In order to ensure better results, however, similar fine grid is used for the detailed impeller model.



(a) The impeller



(b) The simplified impeller in the model



(c) detailed impeller (CAD) in the model

Figure 3: The dredging impeller in practice and in the CFD model.

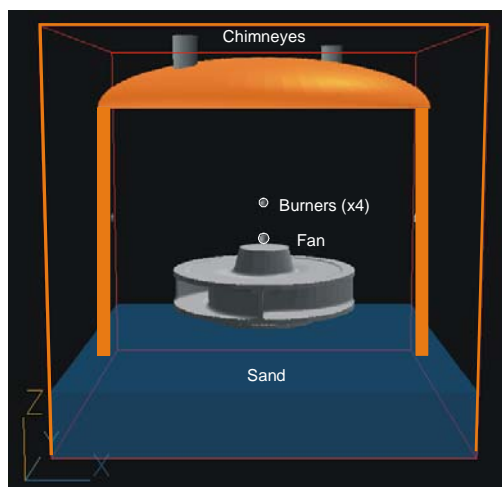


Figure 4: Geometry and the objects in the CFD model.

Besides the discretisation of space coordinates, the time of furnace operation is divided into 55 time-steps for the total of 20 hours. In order to catch the sharp flow and temperature changes in the starting period, time steps of 2, 10, 30, 60 seconds have been used for the first 5 minutes, later 5 and 10 minutes till 30 minutes, and 30 minutes for the rest period between 30 minutes and 20 hours. Because of the long computational time, finer time-steps could not be tested for such a long transient operation.

Summary of the Key Model Parameters

Table 2 lists the general model parameters and boundary conditions for the simulation. Table 3 gives the thermal physical properties of the combustion gas system. The properties of the fuel are estimated from the oil properties and under assumption that all the oil has been vaporized upon entering the furnace.

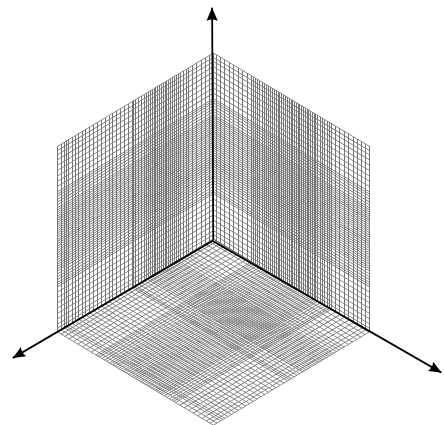


Figure 5: The Cartesian grid of 59×59×54 cells.

Parameters	Value	Parameters	Value
Fuel/air input at burners		Emissivity of the impeller	0.80
Inlet temperature	30°C	Gas absorption coefficient	0.10 m ⁻¹
Inlet velocity	10.12 m/s	Gas scattering coefficient	0.001 m ⁻¹
Tangential velocity	1.15 m/s (6.5°)	Outer wall temperature	50°C
Fuel mass flow rate	0.00255 kg/s	Inner wall emissivity	0.80
Air mass flow rate	0.0908 kg/s	Wall – gas interactions	Log-law wall function
Fuel mass fraction	0.0273	Turbulence intensity at inlet	5%
Total volume flow rate	1151 Nm ³ /h	k-ε model constants	standard
Heat of combustion	43 MJ/kg	Eddy break-up model constant	25
Stoichiometric ratio	15		

Table 2: Input and boundary condition

Properties	Value
Mixture density	Ideal ideal mixing of 3 gas components
Molecular weight	
Fuel (estimated from oil)	144 g/mole
Oxidant (air)	29 g/mole
Combustion product	35.7 g/mole
Heat capacity:	mixture heat capacity is proportional to the mass fraction of each species
Fuel	2471 J/kg/K
Oxidant	1110 J/kg/K
Combustion product	1170 J/kg/K
Mixture kinetic viscosity	$1.544 \times 10^{-5} \text{ m}^2/\text{s}$

Table 3: Thermal physical properties of the combustion gas

Model development

The heat transfer from combustion gas to the metal surface, and further to the inner core of the metal, is dominated by many factors such as combustion parameters and burner settings, fuel supply strategy (constant or varying), the quality of radiation model and influence of radiation parameters, rate of excess air in the burners, the model development includes the following models:

- Models with constant fuel supply
- Different fuel supply at different time periods
- Influence of absorption coefficient and emissivity
- Influence of excess air

The simulation results are compared with preset temperature profile of the metal surface. After many testing models, a best set of parameters have been obtained, and the final model is developed. Three heating periods with different oil supply and excess air will predict reasonably well the surface temperature evolution of the impeller. The settings are listed in Table 4, and the prediction of the surface temperature of the impeller is shown in Figure 6. The detailed feature of the final model will be described in the Simulation Results.

Period (hour)	Excess Air (%)	Mixture Fraction	Fuel (kg)	Energy per burner(kW)
0-8	226%	0.02	214	80
8-10.5	160%	0.025	84	100
10.5-20.5	85%	0.035	356	85
Total	-	-	654	-

Table 4: Settings for final model.

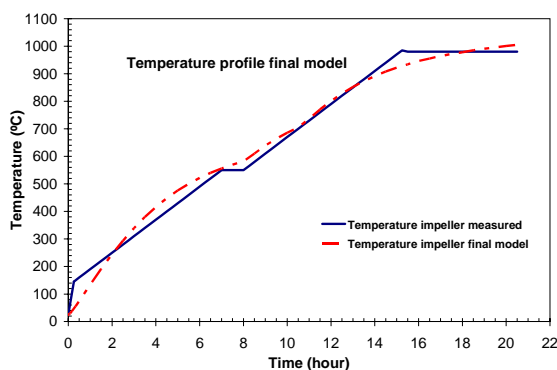


Figure 6: Comparison of the surface temperature profile of the impeller measured and predicted in the final model

In addition, a wide range of gas absorption coefficient (0.05, 0.1, 0.2, 0.4) and surface emissivity of the impeller (0.05, 0.075, 0.1, 0.2, 0.3, 0.5, 0.8, 1.0) have been tested. As an extreme case, a very low absorption coefficient and surface emissivity have been tested for simulating a case of no radiation. It is very clear that radiation heat transfer plays a very important role. However, the change of absorption coefficient between 0.05 and 0.4 does not change appreciably the heat transfer, while the change of surface emissivity of the impeller plays a critical role in the heating profile of the impeller.

The transient simulation has been mainly conducted with HP workstation of 3 GHz running with windows XP. The total computation time varies between 44 and 60 hours for the fine grid of $59 \times 59 \times 54$ (187,974) cells for a total heating period of 20 hours with 55 time steps.

SIMULATION RESULTS

The combustion and metal heating processes are simulated as a time-dependent transient model. In order to compare the end process of the transient heating, steady-state simulations are also conducted. Quite reasonable results are obtained from the simulation. The basic flow feature, the temperature distribution in the combustion space, and the temperature evolution within the impeller are described below.

General Flow Pattern of the Gas Phase

As is described earlier, there are four oil burners installed slightly above the top surface of the impeller. The two opposing burners have a small angle of 6.5° so that the flame jets do not meet in the center of the furnace, and more stable and slightly rotating flames are formed. Figure 7 shows the general gas flow pattern obtained from the final model at three different cross sections. From Figure 6 it can be seen that the jets from the four burners form a counter clockwise rotating flow. This rotating flow extends from the burner level to the top of the furnace upward and to the bottom of the furnace downwards. Near the center of the furnace between the two pair of burners, a downward gas flow is formed, which is ended near the impeller top-surface. Below the impeller the velocity is much lower, which is not efficient for the heating process of the lower part of the impeller.

Owing to the technical and economical limitations, the velocity distribution and the flow pattern have not been validated. Especially the use of standard k-ε model may bring errors to the predicted flow pattern and the turbulence level of the flow. Therefore, more tests with different turbulence models e.g. RNG k-ε model should be made, if the flow visualization cannot be carried out. Perhaps a laboratory scale cold physical models could be used for validating the flow pattern.

Heat Transfer and Temperature Distribution

Based on the combustion heat transfer models with simplified impeller (coarse and fine grid) and the detailed impeller, temperature distribution within the furnace (combustion space) and within the metal impeller is obtained. Energy balance is also made for each case to indicate the energy utilization efficiency, heat loss through the walls. Steady state models are also conducted to verify the end operation of the heat treatment.

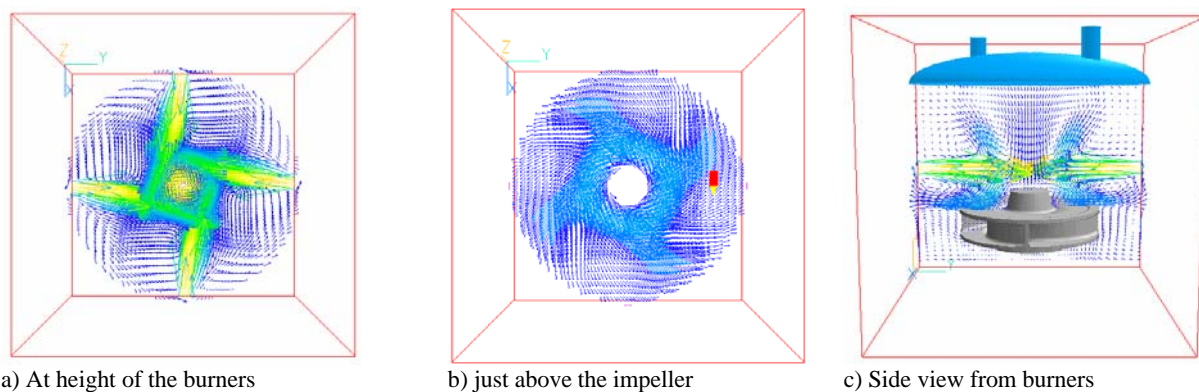


Figure 7: Gas flow pattern in the furnace viewed from different angles

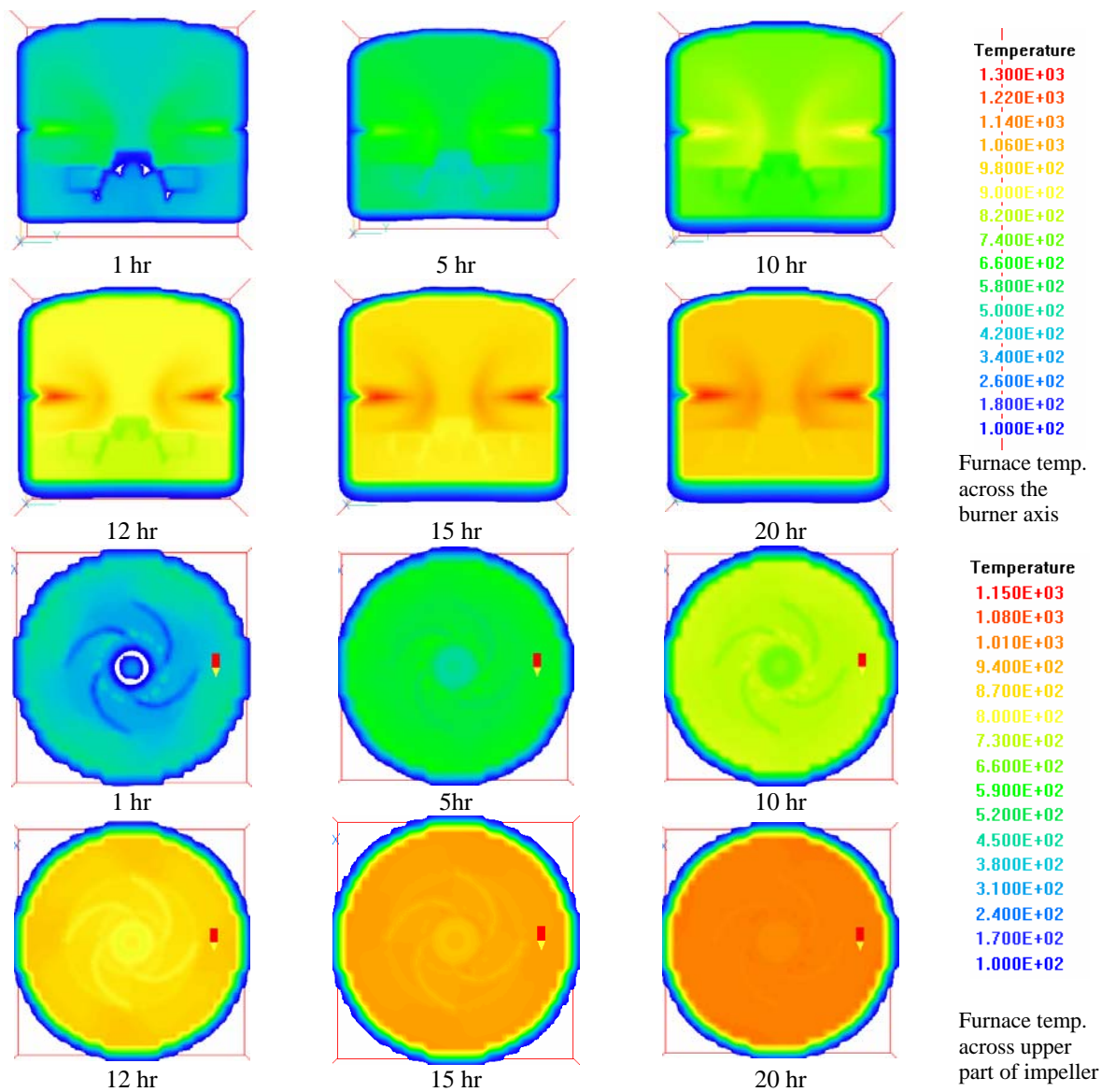


Figure 8: Predicted temperature evolution in the furnace (0 – 20 hours).

Temperature evolution

Figure 8 illustrates a temperature contours from the final transient simulation model. Due to the limited space in the paper, only a few time steps were chosen from the 55 time steps (time 0 – 20.5 hours). From these snap-shots, the heating processes of the furnace space and the impeller can be clearly seen along the heating process. To illustrate more detailed temperature distribution within the dredging impeller, a few temperature maps across middle part of the impeller (blade zone) is also shown in Figure 8. It is clearly shown that the temperature from within the impeller develops slowly.

To get better information of the impeller temperature the outside of the impeller as function of time is analyzed. The temperature is from 180°C to 980°C for the first 15 hours. After sixteen hours the top of the impeller reached the 980°C already. From this point on the temperature scale is set from 920°C till 1020°C, to get a better view of the temperature differences. This is shown in lower part of Figure 8. The temperature of the impeller is higher on the top. The lower parts of the impeller have some delay in temperature increase. As was mentioned before the heating of lower parts is caused mainly by conduction through the metal more than by convection or radiation. The part where the top plate goes over into the blade, the temperature is also slightly lower. The thickness of the impeller may have caused this. Thick parts heat up more slowly than thin parts in general.

In Figure 9 the upper parts of the impeller show higher temperatures. After twenty hours the outside temperature at the top is already more than 1020°C. These figures emphasize the temperature difference between the top and the bottom.

Surface temperature at the end of the heat treatment

At the end the top surface of the impeller has reached to 1050°C whereas the blades are only 970°C (see Figure 10). The surface temperature difference is 90°C. This may cause some internal stresses, which is not favourable for the process. The difference in surface temperature at the end of the process is something, which can be measured in practice as well. This can be done when it really becomes a problem.

Energy distribution

It is important that the energy could be utilized to heat up the metal components more efficiently, under the constraint that the preset heating profile could be maintained. Table 4 illustrates the energy distribution of 4 simulation cases, in which Case D is the final model. The figures show both the first half an hour and at the end of the heat treatment period. Three models show a large difference in the energy carried out by the off-gases. The coarse grid model gives the highest heat loss by the wall, while the two fine grid models predicted similar figure for the wall heat loss of about 11%. Compared to the theoretical calculations for the energy balance, the fine grid model with the detailed impeller predicts the nearest figures for the energy balance.

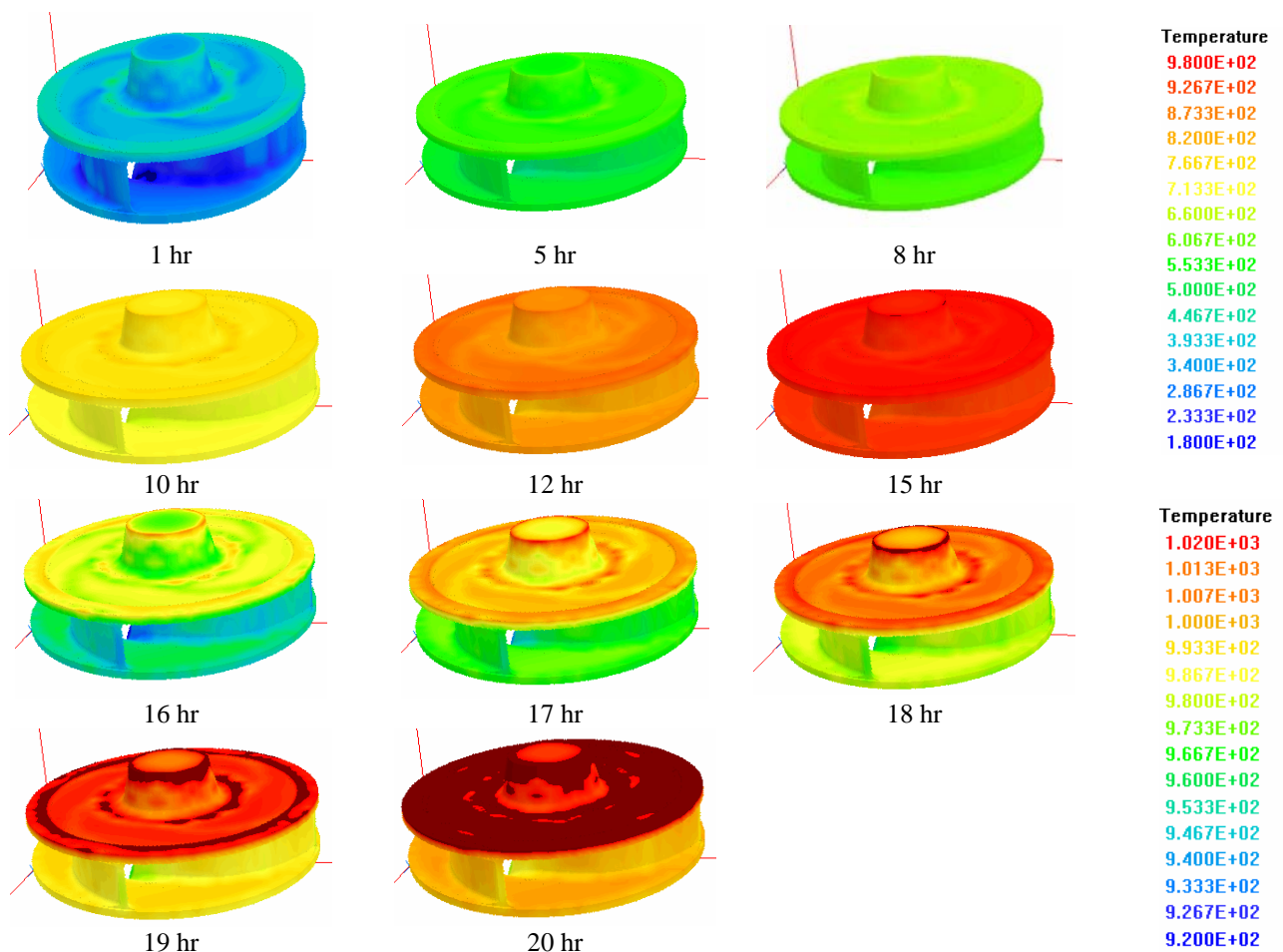


Figure 9: Predicted evolution of the temperature distribution on the surface of the impeller.

Model	Time	Energy input (kW)	Loss to off-gas (%)	Loss to walls (%)	Energy to the metal (%)
A	At 30 min.	512	48.5	5.5	46.0
	At End	512	67.2	27.3	6.6
B	At 30 min.	512	47.0	0	53.0
	At End	512	77.7	11.7	9.6
C	At 30 min.	512	48.0	0	52.0
	At End	512	83.6	10.9	5.5
D	At End operation	340*	74.0	14.7	11.3

Case A: coarse grid with simplified impeller
 Case B: fine grid with simplified impeller
 Case C: fine grid with detailed impeller (CAD)
 Case D: Final model with detailed impeller (CAD) and varying fuel supply.

* In practice and the final model, the fuel supply to the burners is not at constant rate: 0-8 hrs at 320 kW, 8-10.5 hrs at 400 kW, and 10.5 – 20.5 hrs at 340 kW.

Table 4: Energy distribution of the heating process

Figure 11 illustrates the dynamic change of the energy distribution along the heating process for the final model with detailed impeller. It is clear that in the initial heating period the energy from the oil burners is mainly used for metal heating but more than half of the energy leaves the furnace by off-gas. It is also obvious that the energy used for metal heating decreases substantially from about 50% in the beginning to about 20% after 5 hours, and at the end of heating only 11% of energy is used for heating. The wall heat loss increases slowly within the first 2 hours to about 5%, and reaches to about 15% at the end of heat treatment. This distribution feature follows the heat transfer theory, since the energy transported to the metal (and other solid walls) is driven by the temperature difference between the solid and the combustion gas. The wall heat loss is driven by the increasing temperature difference between the outer surface (constant at 50°C) and the inner surface (increasing) of the walls.

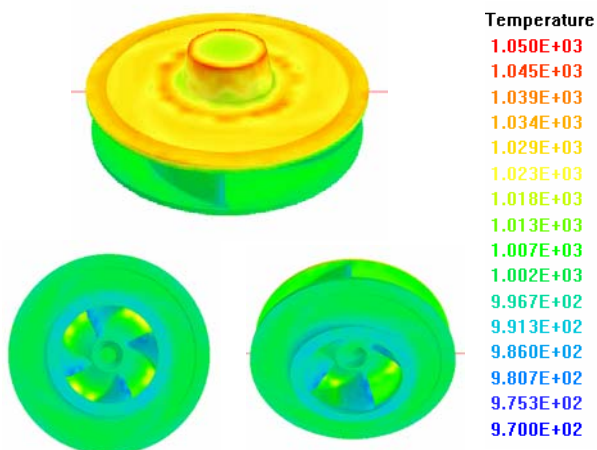


Figure 10: Predicted temperature distribution on the surface of the impeller at the end of operation.

Design alteration: radiation plates

According to the analysis of energy distribution for the current practice, it is found that majority of the energy is lost to the off-gases from fuel combustion. Therefore, energy optimization will be an important aspect to improve. This will result in a decrease in fuel consumption to maintain the required temperature profile, lead to the lower operating costs.

The following alternatives have been investigated:

- Radiation plates
- Heat exchange of off-gas
- Positioning of burners and metal
- Reducing the excess air supply.

Heating of the furnace by means of radiation plates is a good alternative. Preliminary results show that energy efficiency is much higher and production costs can be reduced. This way of heating the furnace is already used in practice at other companies. Figure 12 illustrates the tested configuration and Figure 13 shows the predicted surface temperature profile in 4 periods of energy settings (see Table 5) in comparison with the preset values.

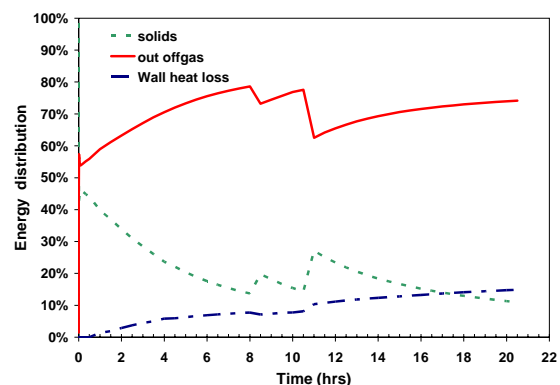


Figure 11: Energy distribution of the final model

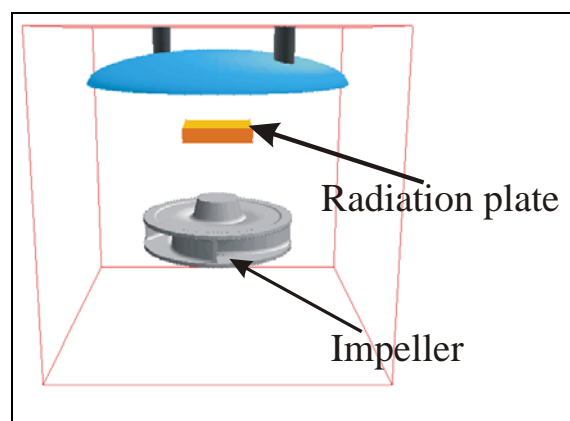


Figure 12: Illustration of the alternative design: radiation plates.

With this total energy consumption of 2233 kWh for the alternative design, the following rough estimation has been made, in comparison with the fuel combustion furnace. The price of 1 kWh in industry is around €0.08. The total energy costs for the radiation plates are then €178. The price of 1 litre of red diesel in industry is € 0.67. The total oil consumption during normal operation is about 774 litre (654 kg), and the total oil costs €520. Thus in stead of €520 only €178 for 2233 kWh electrical energy needs to be paid to heat up the impeller to 980 °C. This is a difference of €342 per heat treatment. To get a better evaluation a cost-benefit analysis has to be made in the future including the purchasing costs of the radiation plates. The placement of the radiation plates has to be examined too to get a more uniform temperature distribution, for instance with plates near the bottom.

Time period	Hours	Energy setting	Total energy
0-2	2	200 constant	400 kWh
2-8	6	75 – 105 kW linear	540 kWh
8-15	7	105 – 150 kW linear	893 kWh
15-20	5	80 constant	400 kWh
Total (0-20)	20		2233 kWh

Table 5: Total energy input for radiation plates

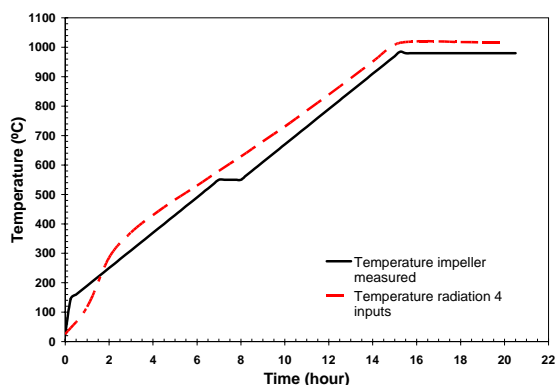


Figure 13: Predicted surface temperature profile by radiation plates heating furnace (4 heating periods with varying energy input).

Other findings of the design changes are as follows. Installation of a heat exchanger will lead to some energy savings but the cost of purchasing the equipment necessary will be too high to get a short return of investment. Positioning of the burners and metal will also improve the energy efficiency but it is expected not to be very high. Finally the reduction of excess air is worth looking into. The reduction of excess air will save a lot of energy and therefore reduce the cost in production. More details of the investigation can be found in the thesis by de Jong (2004).

CONCLUDING REMARKS

This paper presents the CFD simulation of the heating process of a dredging impeller in a cylindrical mobile furnace, by using commercial CFD package PHOENICS. The combustion of the fuel through four oil burners was simulated

with the global turbulent combustion model. The thermal radiation was simulated with the immersed solid (IMMERSOL) radiation model supplied in the code.

The heating profile was reasonably predicted by the simulation. Temperature measurement data was used to validate the CFD model. Through the CFD simulation, not only the surface temperature could be properly predicted, but also the temperature within the metal components could be simulated. The latter is crucial for the heat treatment process, but is not possible to measure directly in practice. Through the simulation it is also found that the energy utilization efficiency is relative low, and the energy is lost substantially by the outgoing off-gas. This indicates that there is large room to improve the energy utilization efficiency.

Various case studies have indicated that by varying the fuel supply to the burners and by regulating the air supply, substantial energy can be saved. Alternatively using radiation plates instead of oil burners can save substantial amount of energy, which is otherwise wasted by the large amount of off-gases. Other options such as the burner orientation and the laying position of the metal component could also reduce to a certain extent the energy consumption.

ACKNOWLEDGEMENTS

The authors would like to thank Mr. J.N.M. Akkermans from Akkermans Gloeitechniek for his interest in this research and for his support to provide process data and temperature measurement. The authors are also grateful for Mr. M.F. Mendes de Leon from IHC for his interests in the project and constructive suggestions to this work.

REFERENCES

- Cham, PHOENICS: Parabolic Hyperbolic Or Elliptic Numerical Integration Code Series, <http://www.cham.co.uk> (accessed in December 2004)
- De Jong., R.A. (2004), Modelling of a Heat Treatment Furnace. Msc. Thesis, Delft University of Technology. GT2004A10. 133 p.
- Spalding, D. B. (1979), Combustion and Mass Transfer, Pergamon Press: Oxford., 409 p.
- Y. Yang, R. A. de Jong and M.A. Reuter (2004), "Simulation of combustion and metal heating in a mobile heat treatment furnace", Multiphase Phenomena and CFD Modeling and Simulation of Engineering Processes, eds. Laurentiu Nastac and Ben Q. Li, TMS Annual Meeting, March 14-18, 2004 Charlotte, North Carolina. TMS, Warrendale. p. 429-439.